

# ALGAN: Anomaly Detection by Generating Pseudo Anomalous Data via Latent Variables

Hironori Murase,<sup>1</sup> Kenji Fukumizu,<sup>2,1</sup>

<sup>1</sup> The Graduate University for Advanced Studies, SOKENDAI

<sup>2</sup> The Institute of Statistical Mathematics

h-murase@ism.ac.jp, fukumizu@ism.ac.jp

## Abstract

In many anomaly detection tasks, where anomalous data rarely appear and are difficult to collect, training with only normal data is important. Although it is possible to manually create anomalous data using prior knowledge, they may be subject to user bias. In this paper, we propose an Anomalous Latent variable Generative Adversarial Network (ALGAN) in which the GAN generator produces pseudo-anomalous data as well as fake-normal data, whereas the discriminator is trained to distinguish between normal and pseudo-anomalous data. This differs from the standard GAN discriminator, which specializes in classifying two similar classes. The training dataset contains only normal data as anomalous states are introduced in the latent variable and input them into the generator to produce diverse pseudo-anomalous data. We compared the performance of ALGAN with other existing methods using the MVTec-AD, Magnetic Tile Defects, and COIL-100 datasets. The experimental results showed that the proposed ALGAN exhibited an AUROC comparable to state-of-the-art methods while achieving a much faster prediction time.

## 1 Introduction

Anomaly detection is a technique that distinguishes between unexpected and normal data and is closely related to outlier detection and novelty detection (Chandola, Banerjee, and Kumar 2009). Applications include fraud detection, medical diagnosis, surveillance, and optical inspection (Ruff et al. 2021; Chalapathy and Chawla 2019; Chandola, Banerjee, and Kumar 2009). The difficulty with anomaly detection is that, in many cases, anomalous data are rarely observed and of a wide variety; hence, the learning of anomaly detection models suffers from the difficulty of imbalanced or one-class classification (e.g., (Perales Gómez et al. 2019; Rodda and Erothi 2016; Chalapathy, Menon, and Chawla 2018)). While some studies have considered the augmentation of anomalous data from different sources (Kawachi, Koizumi, and Harada 2018; Hendrycks, Mazeika, and Dietterich 2018), undesired biases may be introduced.

This paper discusses anomaly detection using only normal training data. Because preparing a large amount of anomalous data is difficult, training without anomalous data is a preferable approach. In this line of research, a wide variety of methods have already been proposed based on traditional machine learning and statistical techniques, such as

one-class classification, likelihood, nearest neighbors, and clustering. See (Chandola, Banerjee, and Kumar 2009) for a comprehensive survey of the traditional approaches.

Recently, deep learning methods such as representation learning and deep generative models have been successfully applied to anomaly detection without using anomalous data for training (Chalapathy and Chawla 2019; Ruff et al. 2021; Pang et al. 2021). Taking advantage of the effective representation of deep learning, the features obtained by a pre-trained model, such as VGG (Simonyan and Zisserman 2015) and ResNet (He et al. 2016), are applied to unsupervised anomaly detection (Andrews et al. 2016). Because Generative Adversarial Networks (GANs, (Goodfellow et al. 2014)) can learn a generative model of normal data through a discrimination task, they have been combined for anomaly detection in various ways (Schlegl et al. 2017; Zenati et al. 2018; Akçay, Atapour-Abarghouei, and Breckon 2018, 2019; Sabokrou et al. 2018). More details on anomaly detection without using anomalous data for training are discussed in Section 2.

In this paper, we propose a method to improve anomaly detection performance by generating pseudo-anomalous data from only normal training data using GANs. Unlike the standard usage of GANs, the generator of the proposed method provides pseudo-anomalous data as well as fake-normal data, by introducing anomalous states in the latent variable. We call this model Anomalous Latent GAN (ALGAN). Note that the discriminator of a standard GAN is not necessarily suitable for distinguishing between normal and anomalous data. It is trained to discriminate real-normal and fake-normal data such that in successful learning, the two classes are almost similar. By contrast, the discriminator of ALGAN distinguishes between the group of real-normal data and the group of fake-normal and pseudo-anomalous data.

Some state-of-the-art methods of anomaly detection specialize in product appearance inspection from images. For example, DifferNet (Rudolph, Wandt, and Rosenhahn 2021) concatenates feature vectors from three different resolution images and uses them to train the model; PatchCore (Roth et al. 2021) uses hierarchical patches of features to achieve effective and fast performance. These methods presume a pre-trained model and cannot be trained directly from the image data. However, the proposed ALGAN can be trained

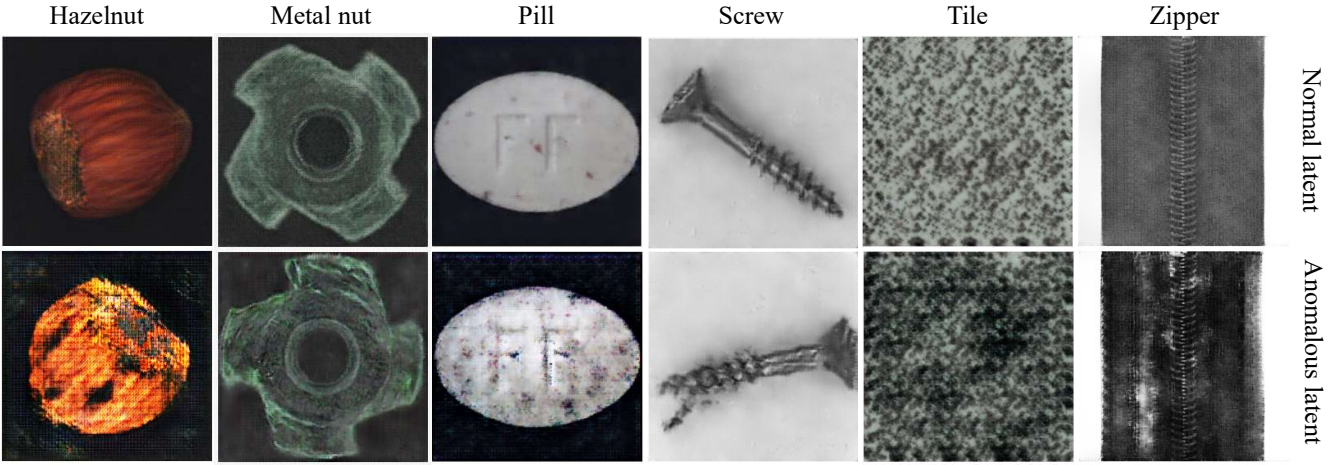


Figure 1: Generated images from ALGAN-image. Top row: Images from normal latent variables  $N(0, I)$ . Bottom row: Images from anomalous latent variables  $N(0, \sigma^2 I)$ , where  $\sigma = 4$  (pseudo-anomalous data).

using both images and features.

To apply anomaly detection in real-world applications, it is important to consider computational resources (Chalapathy and Chawla 2019). Normal training data can be collected efficiently; however, the training time increases with the amount of training data. In addition, real-time prediction is significant in the real world (Sabokrou et al. 2015), where the data generation speed has increased (Ahmad et al. 2017). Reducing computational costs will contribute to expanding the application (Menghani 2021). The proposed ALGAN achieves fast training and prediction times.

The contributions of this study are as follows:

- We propose a novel method for generating pseudo-anomalous data: adding pseudo-anomalous data to GAN training improves the anomaly detection performance of the discriminator.
- The proposed method can be applied to both images and feature vectors. Experimental results showed state-of-the-art performance in image-based methods and comparable ability in feature-based methods.
- The proposed ALGAN achieved a remarkably fast prediction time, 10.4 to 54.6 times faster than other image-based methods on the benchmark MVTec-AD dataset.

This paper is organized as follows. Our work is compared with relevant methods of anomaly detection in Section 2. Section 3 provides preliminaries of standard GANs, details of the proposed method, and intuition for pseudo-anomalous data. In Section 4, the implementation details, datasets, and evaluation method are described; Section 5 examines the anomaly detection performances with various datasets and the results of computation time, stability, and ablation study. Sections 6 and 7 discuss limitations and future work, and conclusion, respectively.

## 2 Related Work

### 2.1 GAN-Based Anomaly Detection

Because a vast body of literature exists on generative models for anomaly detection, we present representative studies using GANs. Anomaly detection methods using GANs can be divided into two categories: those using reconstruction errors and those using one-class classifiers. In early studies (Schlegl et al. 2017; Zenati et al. 2018), the latent variable corresponding to given test data is estimated, and the reconstruction error of the image generated from the latent variable is used as the anomaly score. GANomaly (Akçay, Atapour-Abarghouei, and Breckon 2018) uses two encoders that estimate the latent variables of the input and generated images and detect anomalies using the reconstruction error between two latent variables. Skip-GANomaly (Akçay, Atapour-Abarghouei, and Breckon 2019) is an improvement that evaluates the anomaly score using the features extracted from the middle layer of the discriminator. Because a generator with an encoder-decoder structure trained only on normal data may not properly reconstruct anomalous data, ALOCC (Sabokrou et al. 2018) exploits the one-class classification of the reconstructed images. These methods fail to detect anomalies when data reconstruction is successfully by chance, but the proposed method does not depend on the reconstruction error and discriminates directly.

### 2.2 Anomaly Detection with Pre-Trained Models

Remarkable performance has been demonstrated in recent work (Bergman, Cohen, and Hoshen 2020), which exploits feature representations using models pre-trained on the ImageNet dataset (Deng et al. 2009). The method in (Rippl, Mertens, and Merhof 2021) extracts hierarchical features of normal data from a pre-trained EfficientNet (Tan and Le 2019), fits them with a multivariate normal distribution, and uses the Mahalanobis distance as the anomaly score. SPADE (Cohen and Hoshen 2020) extracts hierarchical features, concatenates them, and performs anomaly detection at

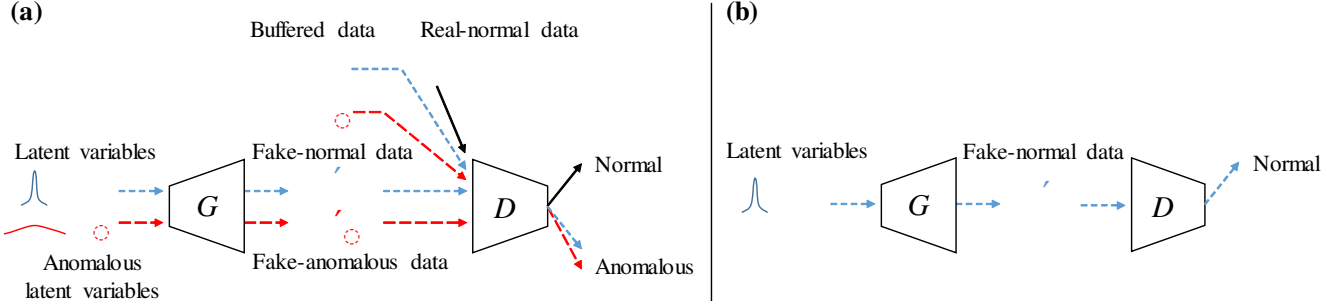


Figure 2: Overview of ALGAN training. (a) Procedure for training the discriminator  $D$  with real-normal data  $x$  (black), latent variables  $z_n \sim N(0, I)$  (blue), latent variables  $z_a \sim N(0, \sigma^2 I)$  (red), fake-normal data  $x'_n$  (blue), fake-anomalous  $x'_a$  (red), buffered fake-normal data  $\hat{x}_n$  (blue) and buffered fake-anomalous data  $\hat{x}_a$  (red). (b) Procedure for training the generator  $G$ .

the image and fine-grained pixel levels using the k-nearest neighbor. PaDiM (Defard et al. 2021) separates hierarchical features into patches and stores the mean and covariance in a memory bank to measure the Mahalanobis distance. PatchCore (Roth et al. 2021) subsamples patches of hierarchical features to achieve a high performance and fast prediction. DifferNet (Rudolph, Wandt, and Rosenhahn 2021) uses a flow-based model (Dinh, Sohl-Dickstein, and Bengio 2017), which typically requires high computational resources, and utilizes pre-trained model (Krizhevsky, Sutskever, and Hinton 2012) features which reduce data dimensionality and computational costs for likelihood-based anomaly detection. Most of these methods use traditional anomaly detection techniques, which require using features, and images cannot be used directly for training. However, the proposed method can use both types of training data.

### 2.3 Pseudo-Anomalous Data

There are some methods that consider the generation of pseudo-anomalous data. Immaturely generated data during the training process of GANs have been used as pseudo-anomalous data for training (Chatillon and Ballester 2020; Zaheer et al. 2020; Pourreza et al. 2021). In CutPaste (Li et al. 2021), patches of random sizes and angles are cut out and randomly pasted onto the image. The classifier is trained either from scratch or fine-tuned using normal and pseudo-anomalous data. The feature representation by the classifier is then used to calculate the anomaly score based on the Gaussian density assumption. The proposed method generates pseudo-anomalous data by introducing anomalous states into latent variables other than using data generated by an immature generator and is less biased than techniques for generating pseudo-anomalous data using prior knowledge.

## 3 Proposed Method

### 3.1 Overview

Figure 2 illustrates the training procedure of our proposed ALGAN. The generator is trained in the same manner as in standard GANs. Two additional data types are employed to train the discriminator. One is generated from the anomalous latent variable, and the other is a buffer of data generated

during the training process. The buffer size is twice as large as the training data, and at each epoch, a portion of the old buffer is replaced with the newly generated data.

### 3.2 Generative Adversarial Networks

GANs (Goodfellow et al. 2014) replace distribution modeling with a discrimination problem: the generator  $G(z; \theta)$  maps latent variables  $z$  to the data space, and the discriminator  $D(x; \phi)$  distinguishes between real data  $x$  and the generated samples  $x' = G(z)$ . When the discriminator can no longer distinguish between real and generated data, the generator approximately realizes a sampler from the real data distribution. The objective function of the GANs is given by

$$\min_G \max_D \left( \mathbb{E}_{x \sim p_{data}(x)} [\log(D(x))] + \mathbb{E}_{z \sim p_z(z)} [\log(1 - D(G(z)))] \right), \quad (1)$$

where  $p_{data}$  and  $p_z$  denote the distributions of real data and latent variables, respectively.

Given the optimal generator, the discriminator can distinguish between two similar classes. Thus, it is nontrivial to determine whether such a discriminator is suitable for identifying real and anomalous data. It has been reported that discriminators perform poorly on anomalous data that are not used for GAN training (Schlegl et al. 2017). This suggests that the discrimination boundary of GANs is not specialized in the one-class classification of anomaly detection.

### 3.3 Pseudo-Anomalous Data

In addition to the training dataset  $\{x\}$  that consists of only real-normal data, ALGAN uses two types of pseudo-anomalous data for the training.

One is generated by anomalous latent variables and is called *fake-anomalous data*. In addition to  $z_n$  following the standard multivariate normal distribution  $N(0, I)$ , which is a common latent for GANs, ALGAN utilizes  $z_a \sim N(0, \sigma^2 I)$  with a larger variance ( $\sigma > 1$ ) to generate pseudo-anomalous data. Variable  $z_a$  is called the anomalous latent variable. See Figure 1 for examples of the pseudo-anomalous images. The generated pseudo-anomalous images

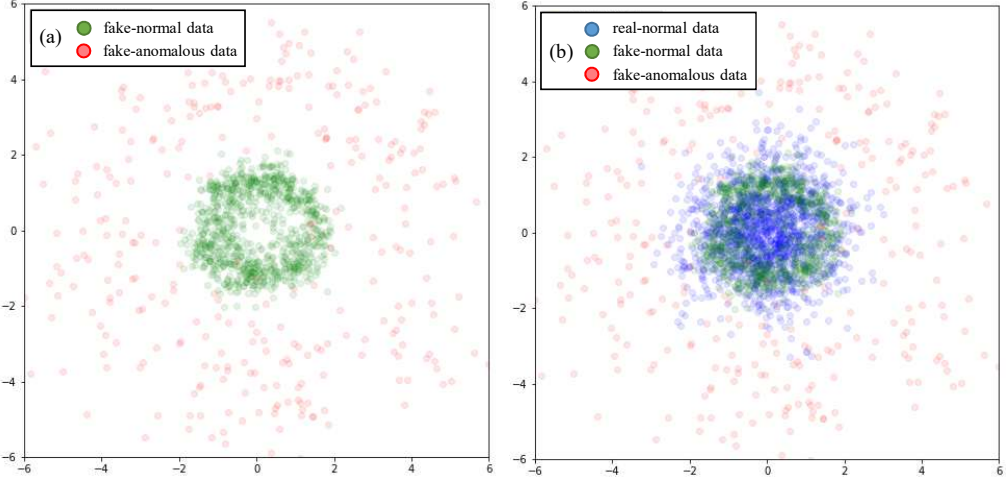


Figure 3: Intuitive interpretation of fake-anomalous data in the toy problem: fake-anomalous data are added to training GANs that map 100-dimensional latent variables to 2-dimensional normal distribution. (a) Fake-anomalous data  $x'_a$  (red) generated by  $\sigma = 4$  are distributed to surround the fake-normal data  $x'_n$  (green). (b) Real-normal data  $x$  (blue) are overlaid on left figure.

are degraded slightly from the normal images. Latent variable  $z$  is a sample from the mixture model.

$$z \sim \alpha N(0, I) + (1 - \alpha)N(0, \sigma^2 I), \quad (2)$$

where  $\alpha$  is the ratio of fake-normal  $x'_n = G(z_n)$  and fake-anomalous  $x'_a = G(z_a)$  data.

The other type of pseudo-anomalous data are called *buffered data*, which are fake samples generated during the early stage of the training process. These are expected to be different from the real-normal data  $x$ . During training, the generated *buffered data*  $\hat{x}_n$  and  $\hat{x}_a$  are buffered and used as pseudo-anomalous data.

### 3.4 Training Methodology

In the training of the discriminator, the real-normal data  $x$  are labeled as *Real*, and the other generated data  $x'_n$ ,  $x'_a$ , and buffered data  $\hat{x}_n$ ,  $\hat{x}_a$  are labeled as *Fake*. Thus, the discriminator of ALGAN learns the discrimination boundary between the real-normal data  $x$  and others. The objective function of ALGAN is given by:

$$\begin{aligned} \min_{G} \max_{D} & \left( \mathbb{E}_x [\log(D(x))] + \alpha \{ \xi \mathbb{E}_{z_n} [\log(1 - D(G(z_n)))] \right. \\ & + (1 - \xi) \mathbb{E}_{\hat{x}_n} [\log(1 - D(\hat{x}_n))] \} \\ & + (1 - \alpha) \{ \xi \mathbb{E}_{z_a} [\log(1 - D(G(z_a)))] \} \\ & \left. + (1 - \xi) \mathbb{E}_{\hat{x}_a} [\log(1 - D(\hat{x}_a))] \} \right), \quad (3) \end{aligned}$$

where  $\xi$  is the ratio of the generated and buffered data. The proposed method followed an adversarial training procedure (Figure 2). It provides a discrimination boundary not only for the real-normal data  $x$  and fake-normal data  $x'_n$  but also for the real-normal  $x$  and pseudo-anomalous data, the latter of which has a broader support of the distribution. As the training progresses, the generator produces data that resemble real-normal data  $x$ , and the discriminator cannot distinguish between real-normal data  $x$  and fake-normal data  $x'_n$ .

The pseudo-anomalous data are clearly different from the real-normal data  $x$ ; therefore, the discrimination boundary of the discriminator is used to classify them. A pseudo-code for the training is presented in Algorithm 1.

Figure 3 and the accompanying movie provide an intuitive understanding of the training for anomaly detection using the fake-anomalous data  $x'_a$ . Fake-normal data  $x'_n$  attempt to approximate the distribution of real-normal data  $x$ , but fake-anomalous data  $x'_a$  are distributed outside of the fake-normal data  $x'_n$ . The discriminator is trained to identify fake-anomalous data  $x'_a$ , even after it can no longer distinguish between real-normal data  $x$  and fake-normal data  $x'_n$ . It provides a discrimination boundary with broader distribution support, and is effective for anomaly detection.

### 3.5 Anomaly Detection

In ALGAN, the *Real* and *Fake* labels are assigned values of 1 and 0, respectively. The *Real* label corresponds to normal data; thus, the anomaly detection rule is given by

$$\text{ALGAN}(x) = \begin{cases} \text{Normal,} & \text{if } D(x) > \text{threshold,} \\ \text{Anomalous,} & \text{otherwise.} \end{cases} \quad (4)$$

Because the significance of false positives or false negatives depends on their application, the threshold is chosen by the user.

## 4 Experiments

An advantage of ALGAN is that it can be used for both the images and feature vectors extracted from a pre-trained model, whereas some state-of-the-art methods for visual inspection depend on feature vectors (Cohen and Hoshen 2020; Defard et al. 2021; Roth et al. 2021; Rudolph, Wandt, and Rosenhahn 2021). To demonstrate this advantage experimentally, we used two different types of implementation. We call them ALGAN-image and ALGAN-feature, and compare them with the relevant methods.

---

**Algorithm 1: Training algorithm of ALGAN.**


---

**Notation:** Number of batches,  $m$ ; latent variables for  $D$ ,  $z_d$ ; latent variables for  $G$ ,  $z_g$ .  
**Hyperparameters:** Training epochs ( $e$ ), update frequency of latent variables ( $n_z$ ), ratio of normal and anomalous latent variables ( $\alpha$ ), standard deviation of anomalous latent ( $\sigma$ ), and number of updates for  $D$  ( $n_{dis}$ ).

```

1: for  $i = 1, \dots, e$  do
2:   if  $i \bmod n_z = 0$  then
3:     Sample  $z_d \sim \alpha N(0, I) + (1 - \alpha)N(0, \sigma^2 I)$ 
4:     Sample  $z_g \sim N(0, I)$ 
5:   end if
6:   for  $j = 1, \dots, m$  do
7:     Sample  $x \sim p_{data}$ 
8:     for  $k = 1, \dots, n_{dis}$  do
9:        $x' \leftarrow G_\theta(z_d)$ 
10:      if  $i = 1$  then
11:         $Loss_D \leftarrow D_\phi(x) + D_\phi(x')$ 
12:      else
13:        Sample buffered data  $\hat{x} \sim \text{Buffer}$ 
14:         $Loss_D \leftarrow D_\phi(x) + D_\phi(x') + D_\phi(\hat{x})$ 
15:      end if
16:       $\phi \leftarrow Adam(Loss_D, \phi)$ 
17:    end for
18:    Buffer  $\leftarrow x'$ 
19:     $Loss_G \leftarrow D_\phi(G_\theta(z_g))$ 
20:     $\theta \leftarrow Adam(Loss_G, \theta)$ 
21:  end for
22: end for
23: return  $D_\phi, G_\theta$ 

```

---

## 4.1 Implementation Details

**Network Architecture and Hyperparameter** ALGAN-image employs an architecture similar to that of DCGAN (Radford, Metz, and Chintala 2016). The generator and discriminator use seven transposed convolutional and convolutional layers, respectively.

For ALGAN-feature, WideResNet101 (Zagoruyko and Komodakis 2016) is applied to the feature extractor to obtain 2048-dimensional vectors from the last block with global average pooling. Both the generator and discriminator have three fully connected layers.

In both architectures, the generator uses batch normalization (Ioffe and Szegedy 2015) and the ReLU activation function, while batch normalization is removed from the output layer. The discriminator employs spectral normalization (Miyato et al. 2018) and the Leaky-ReLU activation function.

The networks were optimized using Adam (Kingma and Ba 2015) with momentum  $\beta_1 = 0$  and  $\beta_2 = 0.9$ , and the learning rates of the generator and discriminator were set to  $2 \times 10^{-4}$  and  $1 \times 10^{-4}$ , respectively. The latent variable  $z$  had 100 dimensions and the standard deviation of the anomalous latent variable used  $\sigma = 4$ . The parameters that determine the ratio of the pseudo-anomalous data were set to  $\alpha = 0.75$  and  $\xi = 0.75$ . The parameters of Algorithm 1 applied  $n_z = 2$  and  $n_{dis} = 2$ . The buffer holds twice the batch size, half

of which is randomly replaced by newly generated data.

The comparison methods were implemented using a DCGAN-like architecture similar to ALGAN-image. In GANomaly (Akçay, Atapour-Abarghouei, and Breckon 2018) and Skip-GANomaly (Akçay, Atapour-Abarghouei, and Breckon 2019), the dimensions of the latent variables were set 100 and 512, respectively. The image resolution for each method was used  $256 \times 256$ . All the experiments were trained using a batch size of 16.

**Software and Hardware** All experiments were implemented in Python 3.8.8 and PyTorch 1.8.1 on Ubuntu 20.04 LTS. An AMD EPYC 7542 32-core processor with 512 GB memory and NVIDIA A100-SXM4 40 GB were used for computations.

## 4.2 Datasets

For performance evaluation, we used three different datasets.

**MVTec-AD Dataset** The dataset was designed for visual inspection and consists of 5,354 images, including 5-texture and 10-object categories (Bergmann et al. 2019). The training set contains 3,629 defect-free (normal) images, and the test set contains 467 defect-free (normal) images and 1,258 defective (anomalous) images.

**Magnetic Tile Defects Dataset (MTD)** The dataset consists of grayscale images with different aspect ratios, including 952 defect-free (normal) images and 392 images containing five defect types (anomalous) (Huang, Qiu, and Yuan 2020) (Figure 4).

**COIL-100 Dataset** The dataset contains 100 different object categories and 7,200 images (Nene et al. 1996). Each object category has 72 images rotated every  $5^\circ$  (Figure 4).

**Split into Training and Validation Sets** Because the training set of MVTec-AD and MTD does not contain any defective (anomalous) images, 50% of the test set was used as the validation set, which was used as the stopping rule.

In MTD, no test set are provided separately from the training data; therefore, 50% of the defect-free (normal) images were used for training, the remaining 25% for validation, and 25% for testing.

For COIL-100, 10-categories were selected for normal data and the remaining 90 categories were selected for anomalous data. We used 60% of the normal data as the training set, 20% for validation, 20% for testing, and 50% of the anomalous data for validation and 50% for testing.

**Pre-Processing and Data Augmentation** In MVTec-AD using ALGAN-image, the images were resized to  $256 \times 256$ . To highlight defects, two images are concatenated with the original image and used as an input image: one is created with max pooling and the other with average pooling in the channel axis dimension. For texture categories, vertical and horizontal flips were applied (however, only horizontal flips were applied for wood). In the object categories, vertical flip, horizontal flip, and random rotation were applied to Bottle and Hazelnut. Horizontal flip was applied to Toothbrush, Transistor, and Zipper. Toothbrush was converted into

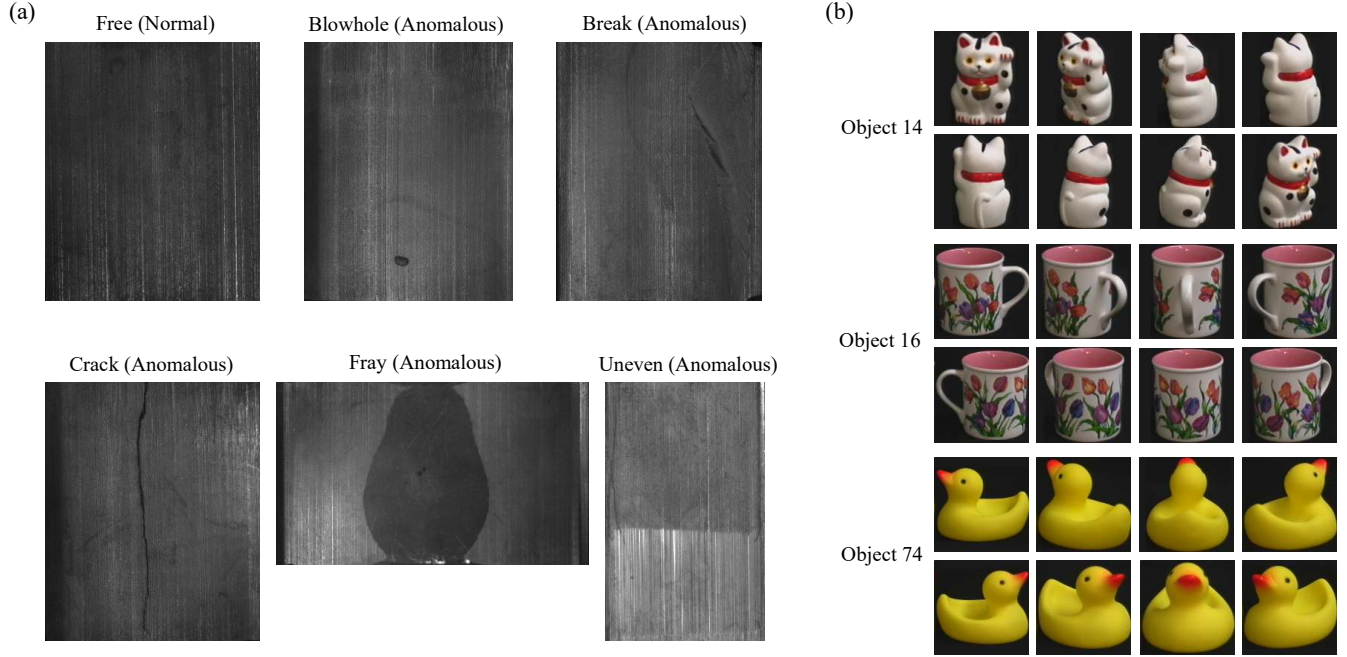


Figure 4: Overview of datasets. (a) Magnetic Tile Defects dataset (MTD) (b) Columbia University Image Library dataset (COIL-100)

grayscale. Metal nut and Screw were applied with random rotation. Cable, Capsule, and Pill were only resized.

In MVTec-AD using ALGAN-feature, texture categories were resized to  $224 \times 224$ . Object categories were resized to  $256 \times 256$ , and then center crops to  $224 \times 224$ . Following Rudolph, Wandt, and Rosenhahn (2021)'s procedure, we applied 24 and 64 different angular rotations during training and prediction, respectively, but using a single-resolution image.

The images of MTD and COIL-100 were resized to  $256 \times 256$  for ALGAN-image and  $224 \times 224$  for ALGAN-feature. For ALGAN-image, a horizontal flip was applied, and for ALGAN-feature, Rudolph, Wandt, and Rosenhahn (2021)'s procedure was applied to both training and prediction.

### 4.3 Evaluation Method and Metric

Accounting for the randomness of the dataset split, we performed 10 experiments with different seed values for each dataset. The performance was evaluated by the area under the receiver operating characteristic (AUROC) curve, which is an area under the curve obtained by moving the classification threshold for the ratio of true-positive and false-positive rates. ALGAN-image is trained for 512 epochs and ALGAN-feature for 192 epochs. The performance was validated every eight epochs on the validation set, and the model that showed the best AUROC was saved. The best model was evaluated on the test set after training.

## 5 Results

### 5.1 Anomaly Detection on MVTec-AD

**Training with Image Data** The results on the test data with the model with the best AUROC for validation (Section 4.3) are shown in Table 1. ALGAN-image significantly outperformed other state-of-the-art image-based methods, such as GANomaly, Skip-GANomaly, and ALOCC. ALGAN-image showed more than 10% higher average accuracy than the others and attained the best accuracy for 13 out of the 15 categories.

**Training with Pre-Trained Features** The results of feature-based methods are listed in Table 2. The results of DifferNet are the means of 10 different test datasets (see Section 4.3). The results of GANomaly were obtained from (Rudolph, Wandt, and Rosenhahn 2021), and the other methods from the respective papers (Cohen and Hoshen 2020; Rippel, Mertens, and Merhof 2021; Defard et al. 2021; Li et al. 2021; Roth et al. 2021). ALGAN-feature shows results comparable to those of DifferNet, whereas PatchCore-25 and CutPaste achieved better performance. Note, however, that the PatchCore and CutPaste methods are specialized strongly for a pre-trained feature.

### 5.2 Anomaly Detection on Other Datasets

The results for MTD and COIL-100 are listed in Tables 3 and 4, respectively. These are the means of 10 trials with the same hyperparameters as those used for the MVTec-AD. ALGAN-image achieved state-of-the-art performance on MTD trained with image data and a comparable result with PatchCore. For MTD, ALGAN-feature performed

Table 1: Results on MVTec-AD. ALGAN-image is compared with methods trained on image data. Top row: mean AUROC. Bottom row: standard deviation. We report the results of 10 experiments using each method. The best performance for each category is indicated in bold font.

	GANomaly	Skip-GANomaly	ALOCC	ALGAN-image
Carpet	0.803	0.829	0.736	<b>0.846</b>
	0.070	0.056	0.054	0.041
Grid	0.924	0.816	0.847	<b>0.938</b>
	0.088	0.079	0.087	0.057
Leather	0.796	0.787	0.768	<b>0.920</b>
	0.079	0.095	0.042	0.041
Tile	0.852	0.941	0.648	<b>0.914</b>
	0.034	0.041	0.071	0.034
Wood	0.939	0.969	0.849	<b>0.972</b>
	0.029	0.020	0.062	0.022
Bottle	0.704	0.674	0.801	<b>0.948</b>
	0.063	0.096	0.075	0.024
Cable	0.686	0.636	0.686	<b>0.877</b>
	0.057	0.064	0.053	0.036
Capsule	0.717	0.691	0.707	<b>0.805</b>
	0.075	0.068	0.073	0.083
Hazelnut	0.765	<b>0.955</b>	0.697	0.836
	0.058	0.036	0.111	0.047
Metal nut	0.698	0.553	0.771	<b>0.811</b>
	0.064	0.105	0.066	0.060
Pill	0.772	0.787	0.659	<b>0.819</b>
	0.050	0.083	0.043	0.053
Screw	0.567	<b>1.000</b>	0.938	0.811
	0.357	0.001	0.076	0.090
Toothbrush	0.774	0.808	0.778	<b>0.933</b>
	0.098	0.084	0.102	0.048
Transistor	0.783	0.769	0.745	<b>0.865</b>
	0.067	0.094	0.085	0.074
Zipper	0.693	0.675	0.656	<b>0.879</b>
	0.052	0.070	0.079	0.025
mean	0.765	0.793	0.752	<b>0.878</b>

worse than ALGAN-image. This may be because the features useful for anomaly detection could not be extracted from the last block of WideResNet-101. Because the features from the deep block in ResNet are biased towards ImageNet (Roth et al. 2021), the features from the shallow block should be used to identify more abstract features required for MTD. For the COIL-100 benchmark, all the methods performed almost perfectly.

Figure 5 shows the histogram of the raw output values of the discriminator before it is input into the sigmoid function of ALGAN-image. The distributions of normal and anomalous data are significantly separated. In COIL-100, normal

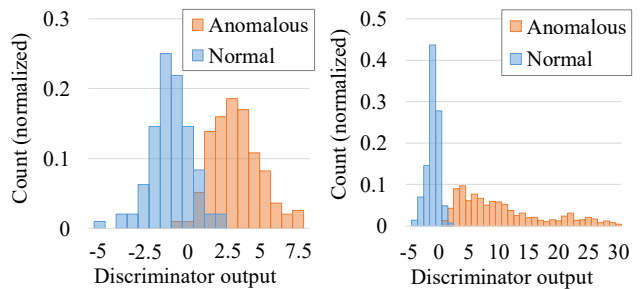


Figure 5: Histograms of raw output values of the discriminator before input to the sigmoid function in ALGAN-image. Left: Magnetic Tile Defects. Right: COIL-100. The sign is reversed so that the horizontal axis represents the anomaly score.

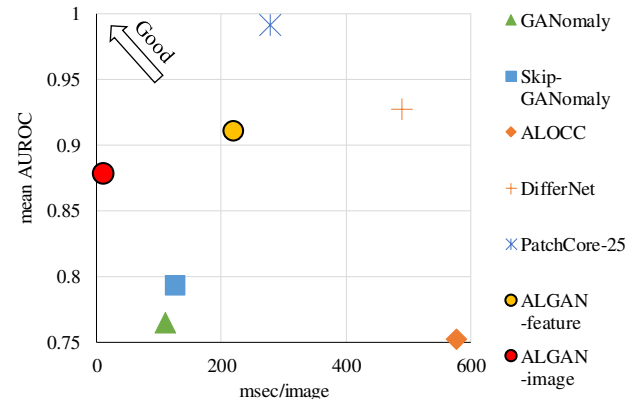


Figure 6: Mean AUROC vs. prediction time for each method on MVTec-AD.

data have a peaky distribution with fewer variations, while the distribution of anomalous data shows a long tail, reflecting the large variations of anomalous data.

### 5.3 Prediction and Training Time

Table 5 shows results comparing the prediction time for MVTec-AD. We can see that ALGAN-image achieved the significantly fastest prediction time (10.6 msec), which is 10.4 to 54.6 times faster than the other image-based methods. ALGAN-feature is 1.3 to 2.2 times faster than the other methods trained on the feature. Figure 6 depicts the prediction time and AUROC performance of the selected methods. ALGAN-image is the fastest and has a high AUROC, but it is not the highest. ALGAN-feature is faster than the other feature-based methods while maintaining a competitive AUROC. With the fast prediction of ALGAN-image, it can be applied to expensive tasks such as real-time prediction with a large number of bounding boxes obtained from object detection (Liu et al. 2020).

A comparison of the training times on MVTec-AD is presented in Table 6. ALGAN-image is the fastest among the compared methods, with the default number of epochs described in Section 4.3. Because there is no official im-

Table 2: Results on MVTec-AD. ALGAN-feature is compared with methods learned from features of pre-trained models. For DifferNet and ALGAN-feature, we report the mean AUROC results of 10 experiments. The best performance for each category is indicated in bold font.

	SPADE	Mah.AD	PaDiM	CutPaste	PatchCore-25	GANomaly	DifferNet	ALGAN-feature
Texture	-	0.978	0.990	0.962	<b>0.991</b>	0.775	0.915	0.925
Object	-	0.950	0.972	0.955	<b>0.992</b>	0.755	0.934	0.905
ALL	0.855	0.958	0.979	0.961	<b>0.991</b>	0.761	0.927	0.911

Table 3: Results on Magnetic Tile Defects. For training with the image data, we report the mean AUROC results of 10 experiments. Numbers in bold indicate the best performance.

	Training with image data			Training with pre-trained features			
	GANomaly	Skip-GANomaly	ALGAN-image	PatchCore-10	GANomaly-feat.	DifferNet	ALGAN-feature
AUROC	0.683	0.504	<b>0.956</b>	<b>0.979</b>	0.766	0.977	0.824

Table 4: Results on COIL-100. Top row: mean AUROC. Bottom row: standard deviation. We report the results of 10 experiments using each method. The best performance is in bold.

	DifferNet	PatchCore-1	ALGAN-image	ALGAN-feature
AUROC	0.999	<b>1.000</b>	0.999	<b>1.000</b>

lementation of PatchCore, we did not use the Faiss library (Johnson, Douze, and Jégou 2021)<sup>1</sup>, which is used in the original study, but applied our own implementation.

#### 5.4 Training Stability

Zaheer, Lee, Astrid, and Lee (2020) have reported that GAN-based anomaly detection exhibited unstable validation results during the training process (Zaheer et al. 2020). Upon validation, our proposed method showed stable results in terms of AUROC (Figure 7).

#### 5.5 Ablation Study

Ablation studies were performed to verify the effect of the two types of pseudo-anomalous data on performance. In ALGAN, buffered data and the data generated by anomalous latent variables were used as pseudo-anomalous data. The checkmark in Table 7 indicates the type(s) used. While either of the two improves the performance, using both works best and reduces the variance. These results validate the usefulness of the proposed method in obtaining pseudo-anomalous data.

<sup>1</sup>Our implementation uses the scikit-learn (Pedregosa et al. 2011) library for core-set selection (Sener and Savarese 2018) and random projection (Sinha et al. 2020). We confirmed that our implementation produces an AUROC similar to the results in (Roth et al. 2021).

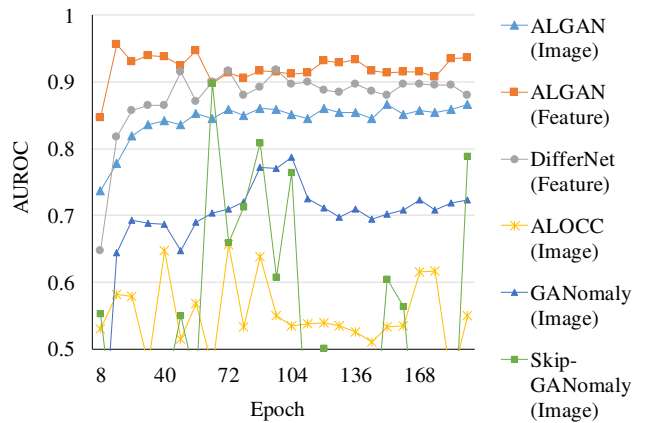


Figure 7: Validation results were plotted every 8 epochs during the training of the transistor category. ALGAN-image and ALGAN-feature show stable AUROCs compared with other GAN-based methods.

## 6 Limitations and Future Work

The hyperparameter for the anomalous latent variables used  $\sigma = 4$  and other possibilities were not comprehensively reported in this study. In some additional experiments, we observed that changing the value of  $\sigma$  or changing the distribution of the anomalous latent variables (e.g., uniform distribution) showed good results. The pursuit of effective methods for defining latent distributions is an interesting topic for future research.

In contrast to state-of-the-art methods for visual inspection tasks, such as PatchCore (Roth et al. 2021), the proposed method, ALGAN, can be applied to any type of data owing to the potential of GAN, which can learn any type of distribution. While the evaluation in this study focused on image data, it will be interesting to see the performance of ALGAN for anomaly or novelty detection in other data types, such as signals (Brophy et al. 2021) and text (de Rosa and Papa 2021). This is an important topic for future work.

Table 5: Mean prediction time per single test image for all categories on MVTec-AD. Bold font indicates the best result.

	GANomaly	Skip-GANomaly	ALOCC	DifferNet	PatchCore-25	ALGAN-feature	ALGAN-image
msec/image	109.8	126.3	577.8	489.5	278.6	218.9	<b>10.6</b>

Table 6: Mean training time for all categories on MVTec-AD. Bold font indicates the best result.

	GANomaly	Skip-GANomaly	ALOCC	DifferNet	PatchCore-25	ALGAN-feature	ALGAN-image
Training Epochs	512	512	512	192	-	196	512
Training Time (min)	23	47	401	55	98	41	<b>22</b>

Table 7: Ablation study results on MVTec-AD with ALGAN-image. Each experiment was conducted 10 times. The left side of the mean AUROC column shows the mean and the right side shows the standard deviation. The best performance is in bold.

Buffered Data	Anomalous Latent	Mean AUROC	
✓		0.643	0.097
		0.761	0.102
	✓	0.779	0.104
✓	✓	<b>0.878</b>	0.049

## 7 Conclusion

We proposed a novel GAN-based anomaly detection method called ALGAN. The ALGAN generator provides pseudo-anomalous data as well as fake-normal data, by introducing anomalous states in the latent variable. The discriminator of ALGAN distinguishes between the group of real-normal data and the group of fake-normal and pseudo-anomalous data.

The proposed method for generating pseudo-anomalous data can be applied to both images and feature vectors. We applied it to three anomaly detection benchmarks and demonstrated its high accuracy.

On MVTec-AD, ALGAN-image achieved more than 10% higher average accuracy than the other image-based methods, and ALGAN-feature has comparable ability to feature-based methods. On the COIL-100 dataset, ALGAN performed almost perfectly.

ALGAN shows remarkably fast predictions. Compared with methods trained on image data and the feature, ALGAN-image can predict 10.4 to 54.6 times faster while maintaining high performance, and ALGAN-feature can predict 1.3 to 2.2 times faster.

## References

Ahmad, S.; Lavin, A.; Purdy, S.; and Agha, Z. 2017. Unsupervised real-time anomaly detection for streaming data. *Neurocomputing*, 262: 134–147.

Akçay, S.; Atapour-Abarghouei, A.; and Breckon, T. P. 2018. Ganomaly: Semi-supervised anomaly detection via adversarial training. In *Asian Conference on Computer Vision*, 622–637. Springer.

Akçay, S.; Atapour-Abarghouei, A.; and Breckon, T. P. 2019. Skip-ganomaly: Skip connected and adversarially trained encoder-decoder anomaly detection. In *2019 International Joint Conference on Neural Networks (IJCNN)*, 1–8. IEEE.

Andrews, J.; Tanay, T.; Morton, E. J.; and Griffin, L. D. 2016. Transfer representation-learning for anomaly detection. In *ICML 2016, Anomaly Detection Workshop*.

Bergman, L.; Cohen, N.; and Hoshen, Y. 2020. Deep nearest neighbor anomaly detection. *arXiv preprint arXiv:2002.10445*.

Bergmann, P.; Fauser, M.; Sattlegger, D.; and Steger, C. 2019. MVTec AD—A Comprehensive Real-World Dataset for Unsupervised Anomaly Detection. In *Conference on Computer Vision and Pattern Recognition*, 9592–9600.

Brophy, E.; Wang, Z.; She, Q.; and Ward, T. 2021. Generative adversarial networks in time series: A survey and taxonomy. *arXiv preprint arXiv:2107.11098*.

Chalapathy, R.; and Chawla, S. 2019. Deep learning for anomaly detection: A survey. *arXiv preprint arXiv:1901.03407*.

Chalapathy, R.; Menon, A. K.; and Chawla, S. 2018. Anomaly detection using one-class neural networks. *arXiv preprint arXiv:1802.06360*.

Chandola, V.; Banerjee, A.; and Kumar, V. 2009. Anomaly Detection: A Survey. *ACM Computing Surveys*, 41(3).

Chatillon, P.; and Ballester, C. 2020. History-based anomaly detector: an adversarial approach to anomaly detection. In *Proceedings of SAI Intelligent Systems Conference*, 761–776. Springer.

Cohen, N.; and Hoshen, Y. 2020. Sub-image anomaly detection with deep pyramid correspondences. *arXiv preprint arXiv:2005.02357*.

de Rosa, G. H.; and Papa, J. P. 2021. A survey on text generation using generative adversarial networks. *Pattern Recognition*, 119: 108098.

Defard, T.; Setkov, A.; Loesch, A.; and Audigier, R. 2021. PaDiM: A patch distribution modeling framework for anomaly detection and localization. In *International Conference on Pattern Recognition*, 475–489. Springer.

Deng, J.; Dong, W.; Socher, R.; Li, L.-J.; Li, K.; and Fei-Fei, L. 2009. Imagenet: A large-scale hierarchical image database. In *Conference on Computer Vision and Pattern Recognition*, 248–255. IEEE.

Dinh, L.; Sohl-Dickstein, J.; and Bengio, S. 2017. Density estimation using Real NVP. In *International Conference on Learning Representations*.

Goodfellow, I.; Pouget-Abadie, J.; Mirza, M.; Xu, B.; Warde-Farley, D.; Ozair, S.; Courville, A.; and Bengio, Y. 2014. Generative adversarial nets. In *Advances in Neural Information Processing Systems*, 2672–2680.

He, K.; Zhang, X.; Ren, S.; and Sun, J. 2016. Deep residual learning for image recognition. In *Conference on Computer Vision and Pattern Recognition*, 770–778.

Hendrycks, D.; Mazeika, M.; and Dietterich, T. 2018. Deep Anomaly Detection with Outlier Exposure. In *International Conference on Learning Representations*.

Huang, Y.; Qiu, C.; and Yuan, K. 2020. Surface defect saliency of magnetic tile. *The Visual Computer*, 36(1): 85–96.

Ioffe, S.; and Szegedy, C. 2015. Batch Normalization: Accelerating Deep Network Training by Reducing Internal Covariate Shift. In *International Conference on Machine Learning*, 448–456.

Johnson, J.; Douze, M.; and Jégou, H. 2021. Billion-scale similarity search with gpus. *IEEE Transactions on Big Data*, 7(3): 535–547.

Kawachi, Y.; Koizumi, Y.; and Harada, N. 2018. Complementary set variational autoencoder for supervised anomaly detection. In *International Conference on Acoustics, Speech and Signal Processing*, 2366–2370. IEEE.

Kingma, D. P.; and Ba, J. 2015. Adam: A method for stochastic optimization. In *International Conference on Learning Representations*.

Krizhevsky, A.; Sutskever, I.; and Hinton, G. E. 2012. ImageNet Classification with Deep Convolutional Neural Networks. In *Advances in Neural Information Processing Systems*, volume 25, 1097–1105.

Li, C.-L.; Sohn, K.; Yoon, J.; and Pfister, T. 2021. CutPaste: Self-Supervised Learning for Anomaly Detection and Localization. In *Conference on Computer Vision and Pattern Recognition*, 9664–9674.

Liu, L.; Ouyang, W.; Wang, X.; Fieguth, P.; Chen, J.; Liu, X.; and Pietikäinen, M. 2020. Deep learning for generic object detection: A survey. *International Journal of Computer Vision*, 128(2): 261–318.

Menghani, G. 2021. Efficient Deep Learning: A Survey on Making Deep Learning Models Smaller, Faster, and Better. *arXiv preprint arXiv:2106.08962*.

Miyato, T.; Kataoka, T.; Koyama, M.; and Yoshida, Y. 2018. Spectral Normalization for Generative Adversarial Networks. In *International Conference on Learning Representations*.

Nene, S. A.; Nayar, S. K.; Murase, H.; et al. 1996. Columbia Object Image Library (COIL-100).

Pang, G.; Shen, C.; Cao, L.; and Hengel, A. V. D. 2021. Deep Learning for Anomaly Detection: A Review. *ACM Computing Surveys*, 54(2).

Pedregosa, F.; Varoquaux, G.; Gramfort, A.; Michel, V.; Thirion, B.; Grisel, O.; Blondel, M.; Prettenhofer, P.; Weiss, R.; Dubourg, V.; Vanderplas, J.; Passos, A.; Cournapeau, D.; Brucher, M.; Perrot, M.; and Duchesnay, E. 2011. Scikit-learn: Machine Learning in Python. *Journal of Machine Learning Research*, 12: 2825–2830.

Perales Gómez, A. L.; Fernández Maimó, L.; Huertas Celdrán, A.; García Clemente, F. J.; Cadenas Sarmiento, C.; Del Canto Masa, C. J.; and Méndez Nistal, R. 2019. On the Generation of Anomaly Detection Datasets in Industrial Control Systems. *IEEE Access*, 7: 177460–177473.

Pourreza, M.; Mohammadi, B.; Khaki, M.; Bouindour, S.; Snoussi, H.; and Sabokrou, M. 2021. G2d: Generate to detect anomaly. In *Winter Conference on Applications of Computer Vision*, 2003–2012.

Radford, A.; Metz, L.; and Chintala, S. 2016. Unsupervised Representation Learning with Deep Convolutional Generative Adversarial Networks. In *International Conference on Learning Representations*.

Rippel, O.; Mertens, P.; and Merhof, D. 2021. Modeling the distribution of normal data in pre-trained deep features for anomaly detection. In *International Conference on Pattern Recognition*, 6726–6733. IEEE.

Rodda, S.; and Erothi, U. S. R. 2016. Class imbalance problem in the network intrusion detection systems. In *International Conference on Electrical, Electronics, and Optimization Techniques*, 2685–2688. IEEE.

Roth, K.; Pemula, L.; Zepeda, J.; Schölkopf, B.; Brox, T.; and Gehler, P. 2021. Towards Total Recall in Industrial Anomaly Detection. *arXiv preprint arXiv:2106.08265*.

Rudolph, M.; Wandt, B.; and Rosenhahn, B. 2021. Same Same But DifferNet: Semi-Supervised Defect Detection with Normalizing Flows. In *Winter Conference on Applications of Computer Vision*.

Ruff, L.; Kauffmann, J. R.; Vandermeulen, R. A.; Montavon, G.; Samek, W.; Kloft, M.; Dietterich, T. G.; and Müller, K.-R. 2021. A Unifying Review of Deep and Shallow Anomaly Detection. *Proceedings of the IEEE*, 109(5): 756–795.

Sabokrou, M.; Fathy, M.; Hoseini, M.; and Klette, R. 2015. Real-time anomaly detection and localization in crowded scenes. In *Proceedings of the IEEE conference on computer vision and pattern recognition workshops*, 56–62.

Sabokrou, M.; Khalooei, M.; Fathy, M.; and Adeli, E. 2018. Adversarially learned one-class classifier for novelty detection. In *Conference on Computer Vision and Pattern Recognition*, 3379–3388.

Schlegl, T.; Seeböck, P.; Waldstein, S. M.; Schmidt-Erfurth, U.; and Langs, G. 2017. Unsupervised anomaly detection

with generative adversarial networks to guide marker discovery. In *International Conference on Information Processing in Medical Imaging*, 146–157. Springer.

Sener, O.; and Savarese, S. 2018. Active Learning for Convolutional Neural Networks: A Core-Set Approach. In *International Conference on Learning Representations*.

Simonyan, K.; and Zisserman, A. 2015. Very Deep Convolutional Networks for Large-Scale Image Recognition. In *International Conference on Learning Representations*.

Sinha, S.; Zhang, H.; Goyal, A.; Bengio, Y.; Larochelle, H.; and Odena, A. 2020. Small-gan: Speeding up gan training using core-sets. In *International Conference on Machine Learning*, 9005–9015. PMLR.

Tan, M.; and Le, Q. 2019. Efficientnet: Rethinking model scaling for convolutional neural networks. In *International Conference on Machine Learning*, 6105–6114. PMLR.

Zagoruyko, S.; and Komodakis, N. 2016. Wide Residual Networks. In *British Machine Vision Conference*. British Machine Vision Association.

Zaheer, M. Z.; Lee, J.-h.; Astrid, M.; and Lee, S.-I. 2020. Old is Gold: Redefining the Adversarially Learned One-Class Classifier Training Paradigm. In *Conference on Computer Vision and Pattern Recognition*, 14183–14193.

Zenati, H.; Foo, C. S.; Lecouat, B.; Manek, G.; and Chandrasekhar, V. R. 2018. Efficient gan-based anomaly detection. *arXiv preprint arXiv:1802.06222*.